WEP Warwick Evans Publishing

Academic Journal of Management Science and Engineering

ISSN: 3080-9827 (Print), ISSN: 3080-9835 (Online) | Volume 1, Number 5, Year 2026
DOI: https://doi.org/10.62051/ajmse.v1n5.01
Journal homepage: https://ajomse.com



Urban Flood Emergency Evacuation Path Optimization Research

Yi Wang, Liang Mao

Sichuan University of Science & Engineering, Zigong, Sichuan, China

ABSTRACT

Existing methods for optimizing urban flood emergency evacuation routes often fail to account for the dynamic evolution of inundation and the heterogeneity of evacuees' ages. To address this gap, this paper proposes a personalized evacuation route optimization approach that integrates Agent-Based Modeling (ABM) with Deep Q-Network (DQN) reinforcement learning. The proposed method incorporates water-depth-dependent speed reduction models and instability thresholds specific to children, adults, and the elderly into both the state space and reward function, enabling DQN to iteratively learn optimal routes that balance safety and efficiency. Using the "7·20" extreme rainstorm in Zhengzhou as a case study, we constructed a 100-year return-period pluvial flooding scenario and conducted evacuation simulations under three activation timings-0, 1, and 2 hours after rainfall onset-comparing the proposed method against the traditional A* algorithm. Results demonstrate that the experimental group reduced average evacuation time by 17.8%-42.1% relative to the control group, with particularly pronounced improvements for children and the elderly (up to 45.1%). The safety metric F-value in the experimental group exceeded that of the control group by more than 0.3 under deep-water conditions and exhibited a more gradual decline. These findings confirm that the DQN-based approach, which integrates age heterogeneity and dynamic water depth, substantially enhances both the timeliness and safety of emergency evacuation during urban floods, offering more reliable route planning for high-risk populations and providing a scientific basis for optimizing urban flood emergency response protocols.

KEYWORDS

Urban Pluvial Flooding; Emergency Evacuation; Route Optimization; Agent-Based Modeling; Deep Reinforcement Learning; Personalized Evacuation.

1. INTRODUCTION

In recent years, under the dual pressures of global climate change and rapid urbanization, the frequency and intensity of extreme precipitation events have continued to escalate, rendering urban rainstorm and flood disasters increasingly severe[1]. The Sixth Assessment Report of the Intergovernmental Panel on Climate Change (IPCC) indicates a marked upward trend in global observed precipitation and heavy rainfall events, with China exhibiting an even more pronounced response to climate change, as evidenced by the sustained rise in both the intensity and frequency of extreme precipitation[2]. Given the high concentration of urban populations and the lagging development of drainage infrastructure relative to the pace of urban expansion, rainstorm-induced flooding frequently results in substantial property losses and casualties[3, 4]. In response, emergency management agencies and researchers have implemented a range of engineering measures—including drainage system maintenance, river dredging, and sponge city construction—alongside enhanced management tools such as disaster forecasting, early warning, simulation, and emergency planning [5, 6], all aimed at safeguarding public safety during extreme events. Nevertheless, owing

Content from this work may be used under the terms of CC BY-NC 4.0 licence (https://creativecommons.org/licenses/by-nc/4.0/).
Published by Warwick Evans Publishing.

to the sudden onset, high destructiveness, and complex evolution of urban flooding, residual risks to human life persist even under extreme conditions[7, 8]. Consequently, devising rational and efficient emergency route planning methods that improve both the safety and timeliness of personnel evacuation is of paramount importance for protecting lives and advancing detailed disaster risk reduction in urban flood management.

Extensive research has been devoted to emergency evacuation route planning in disaster contexts. Li et al. [9]refined the Dijkstra algorithm by incorporating traffic delays and avoiding backtracking, progressively generating more practical and manageable evacuation route plans for flood scenarios. He et al. [10]developed a cellular automaton-based dynamic route optimization algorithm, which, in experiments conducted in a typical study area of Yangzhou, reduced the entrapment rate and average evacuation route length by approximately 32.70% and 34.04%, respectively, compared with the conventional A* algorithm. Yan et al. [11] constructed an emergency evacuation model for a residential district in Shenzhen that balanced efficiency and equity, analyzing the synergistic effects of evacuee population size and sequencing on evacuation performance. Kaynak et al. [12] employed the Dijkstra algorithm to design a route generator that determines optimal vehicle paths, comparing feasible pedestrian routes under both normal and 500-year flood conditions in Waterloo, Iowa. Collectively, these studies provide critical methodological support for pedestrian route planning in flood disasters.

However, existing research suffers from two principal limitations. First, conventional route planning methods typically adopt "shortest distance" or "shortest time" as the sole optimization objective, neglecting the dynamic influence of evolving inundation depths on network traversability and pedestrian safety. Second, significant disparities exist across age groups in terms of both walking capacity and instability thresholds under flooded conditions; children and the elderly exhibit considerably lower stability and markedly slower walking speeds than adults in standing water. Lee et al. [13] demonstrated experimentally that elderly individuals exhibit substantially reduced evacuation speeds relative to younger adults across varying water depths, with the decline becoming more pronounced as depth increases. Nevertheless, the vast majority of emergency evacuation route planning studies employ uniform speed parameters, failing to incorporate age-group-specific mobility differences into routing decisions—a shortcoming that may render planned routes infeasible or even perilous for children and the elderly.

Deep reinforcement learning, particularly the Deep Q-Network (DQN), offers a promising avenue for overcoming these challenges [14]. Unlike traditional route planning algorithms, DQN learns optimal decision policies through trial-and-error interaction with a simulation environment, naturally accommodating dynamic environmental changes and multi-objective optimization. Takabatake et al. [15]combined ABM-based tsunami evacuation simulations with Q-learning to develop individualized evacuation route optimization, achieving notable reductions in casualty rates in a coastal city case study. In the urban flood domain, deep reinforcement learning has also been preliminarily applied to rescue route planning. Nonetheless, the application of reinforcement learning to personalized evacuation route optimization that accounts for age-group differences under urban pluvial flooding conditions remains largely unexplored.

In light of the foregoing, this paper proposes a personalized route optimization methodology for urban rainstorm-induced flooding that couples ABM with DQN. Through iterative refinement of the objective optimization function via DQN, personalized evacuation metrics are constructed that account for agent heterogeneity, safety, and efficiency. The proposed approach is expected to serve as a reference for enhancing the precision and safety of urban flood emergency evacuation.

2. PERSONALIZED EVACUATION ROUTE METHODOLOGY

2.1. Methodological Framework

This study aims to optimize individual evacuation routes by integrating an agent-based flood evacuation simulation model with Q-learning-based deep reinforcement learning, incorporating age-group-specific mobility differences and instability thresholds to construct a personalized evacuation route optimization framework tailored to urban pluvial flooding. The overall architecture of the method is illustrated in Figure 1.

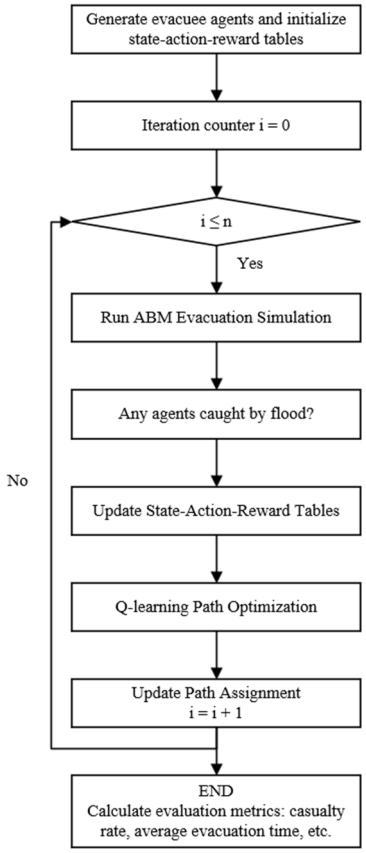


Figure 1. Flowchart of the individual optimal evacuation route computation algorithm

2.1.1. Route Initialization and State–Action–Reward Table Construction.

For each evacuee, an initial route to the nearest shelter is first computed using the A* algorithm, serving as the baseline scheme (iteration 0). Concurrently, an empty state–action–reward table is initialized for each individual.

2.1.2. ABM Evacuation Simulation Execution.

All evacuees move along their currently assigned routes toward shelters. During simulation, individual movement speeds are dynamically computed based on local water depth and age group using the depth-dependent speed reduction model of Bernardini et al. [16]. An individual is deemed to have perished when the water depth at their location exceeds the age-specific instability threshold. The simulation proceeds until all evacuees either reach shelters or are declared deceased.

2.1.3. State–Action–Reward Table Update.

For individuals who perish during a given simulation run, the state–action–reward table is updated based on their actual traversed experience. Actual travel times between road network nodes are recorded, and the reward for reaching a shelter is set to zero.

2.1.4. Q-Learning Update and Route Optimization.

For each perished individual, the DQN algorithm is applied to the state–action–reward table, updating Q-values according to Equation (1) to identify the route scheme that maximizes cumulative reward:

$$Q(s,a) \leftarrow (1-\alpha)Q(s,a)+\alpha(r(s,a)+\gamma \max_{a'} Q(s',a')) \quad (1)$$

Where Q(s,a) denotes the expected cumulative reward of taking action a in state s, r(s,a) is the immediate reward obtained after executing action a,α is the learning rate, and γ is the discount factor. In this study,α=0.01 and γ=0.90.

2.1.5. Iterative Convergence.

The updated route schemes are fed back into the ABM simulation (return to Step 2), and the above process is repeated iteratively. The maximum number of iterations is set to 10 in this study.

2.2. State Space and Reward Function Design

2.2.1. State Space and Action Space.

The state space for each agent encompasses the following information:

$$S=(\text{node_id},t,\text{age_group},\text{water_depth},\text{neighboring_depths}) \quad (2)$$

where node_id is the current node,t is the current time step (0-35),age_group denotes the age category (child/adult/elderly),water_depth and neighboring_depths represent the real-time water depths at the current node and its adjacent nodes, respectively. By incorporating the time step t into the state space, agents can perceive the dynamic progression of flooding and adopt differentiated risk-avoidance strategies at different phases. At road intersections, each agent selects an adjacent node as the next movement target; the action space is defined as the set of all neighboring nodes of the current node.

2.2.2. Reward Function.

The reward function simultaneously addresses both safety and passage efficiency:

$$r(s,a)=R_{safety}+R_{efficiency} \quad (3)$$

Where R_{safety} is assigned a positive reward when the water depth at the target node is below the age-specific instability threshold, and a negative penalty when it exceeds the threshold; $R_{efficiency}$ is computed as the negative value of travel time (i.e., shorter travel time yields higher reward). Through this multi-objective reward function, the DQN algorithm is capable of learning optimal routes that reconcile safety with efficiency.

2.3. Pedestrian Movement Speed and Safety Assurance Mechanisms

2.3.1. Age-Differentiated Pedestrian Movement Speed Settings.

This study categorizes pedestrian movement speeds into three groups: children, adults, and the elderly. The baseline walking speed for children is adopted from Wang et al. [22], who surveyed average crossing speeds of children individuals; for adults, the average walking speed in urban spaces measured by Zhuang et al. [17] is used; for the elderly (aged 65 and above), the average crossing

speed reported by Shirvani et al. [18] is employed. Given that evacuation-induced emotional arousal typically elevates walking speed, experimental evidence indicates that pedestrian speed under excited conditions increases by an average of 68%[19, 20, 21]. Accordingly, the baseline speeds used in this study incorporate the effect of evacuation-related emotional factors. For flooded road surfaces, speed variations with water depth for each age group are computed using the depth-dependent speed reduction model of Bernardini et al. [16].

2.3.2. Age-Differentiated Instability Thresholds.

Considering the increasing risk of pedestrian instability with rising water depth, age-specific instability thresholds are established following Wang et al. [22]: 0.8 m for children, 0.9 m for adults, and 0.8 m for the elderly. When water depth exceeds the respective threshold, the individual's speed is reduced to zero in the velocity model, and a substantial penalty is imposed through the reward function. Additionally, through the safety penalty mechanism embedded in the reward function, DQN enables agents to automatically avoid deep-water segments that pose a threat to their age group, prioritizing routes that ensure safe arrival at shelters. The specific speed configurations are illustrated in Figure 2..

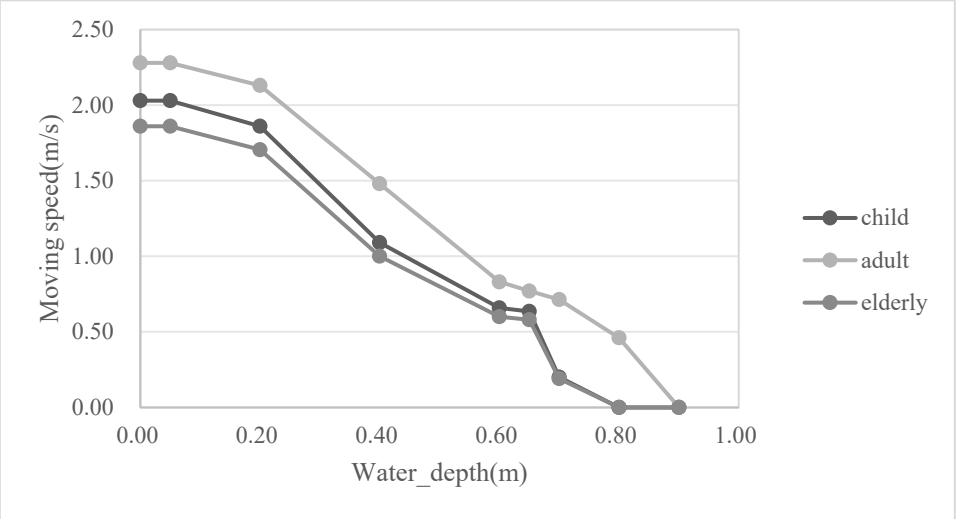


Figure 2. Depth-dependent speed reduction curves for different age groups

3. STUDY AREA AND DATA SOURCES

3.1. Study Area Description

Validating model simulation performance is fundamental to ensuring the reliability of flood inundation projections. This study takes the "7·20" extreme rainstorm and flood disaster in Zhengzhou, Henan Province, as an empirical case, selecting the main urban area of Zhengzhou as the study region. The study area encompasses eight districts of the Zhengzhou central urban area: the five administrative districts of Zhongyuan, Erqi, Jinshui, Guancheng and Huiji, along with the three functional zones of Zhengdong New Area, Economic and Technological Development Zone, and High-Tech Industrial Development Zone. These eight districts form a contiguous spatial unit constituting the most densely populated and economically vibrant core urban area of Zhengzhou, covering approximately 1,078 km². Since 2015, Zhengzhou has experienced rainstorm-induced waterlogging of varying intensities almost annually. On July 20, 2021, an extreme rainfall event struck Zhengzhou, with the maximum hourly rainfall at the national meteorological observation station reaching 201.9 mm—shattering the historical record for hourly rainfall in China's mainland. The disaster resulted in fatalities in the Jingguang Expressway North Tunnel and Metro Line 5, claiming 380 lives and causing direct economic losses of RMB 40.9 billion. The substantial casualties

and property damage inflicted by urban flooding have severely constrained Zhengzhou's sustainable development, underscoring the urgent need for precise and efficient emergency evacuation planning methodologies to mitigate flood losses.

3.2. Data Sources

The data utilized in this study include rainfall records, Digital Elevation Model (DEM), road network data, emergency shelter locations, population distribution data, and time-series water depth data for Zhengzhou. Rainfall data were extracted from the hourly precipitation records for Zhengzhou covering July 19–21, 2021, obtained from the Global Surface Compilation Dataset—Hourly Products published by the National Meteorological Information Center. Terrain data were derived from the 30 m resolution Digital Surface Model (DSM) of Zhengzhou extracted from OpenStreetMap (https://www.openstreetmap.org). Road network data were also extracted from OpenStreetMap and manually calibrated to align with the high-precision terrain of the study area. Emergency shelter data were compiled based on existing emergency shelters in Zhengzhou, supplemented by screening gymnasiums and schools from the national POI database as temporary emergency shelters [26]. Considering spatial accessibility and flood risk, 112 refuge sites were ultimately selected as target evacuation destinations. Population data were obtained from the seventh national population census at the township/subdistrict level. A 100 m grid was employed for spatial population disaggregation across the eight central districts, and overlay analysis was conducted to derive the population counts and age-structure distribution for each grid cell.

3.3. Pluvial Flood Simulation

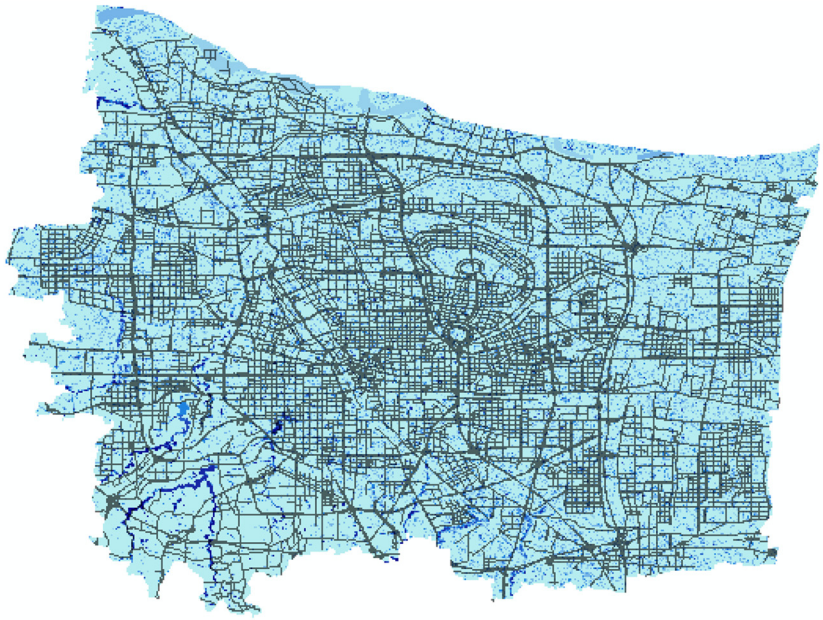


Figure 3. Inundation simulation results for the Zhengzhou "7·20" rainstorm, in meters

This study employs the open-source model SynxFlow [23]to simulate the urban inundation process. Leveraging GPU acceleration, SynxFlow achieves super-real-time computation while maintaining high accuracy (mean water depth deviation < 0.04 m) for large-scale urban areas. Su et al. [24] applied SynxFlow to simulate pluvial flooding scenarios under six return periods ranging from 2 to 100 years in the central urban area of Shenzhen. Model validation using six observed flood events and the "9·7" rainstorm demonstrated a spatial capture rate of flooded points as high as 90.24%, confirming the reliability and efficiency of SynxFlow for urban flood simulation.

In the present study, owing to the lack of detailed drainage network data for Zhengzhou, the municipal design drainage capacity standard (0.2 m/day) was adopted as a substitute. A 100-year return-period design storm was employed as the flood scenario for Zhengzhou. To enhance computational efficiency, the simulation was constrained to the most intense 6-hour rainfall period (15:00–20:00 on July 20). The simulation results are presented in Figure 3, indicating that approximately 63.2% of the main urban area of Zhengzhou experienced inundation. This finding is broadly consistent with the State Council "7·20" investigation report [25], which stated that "more than half of the underground spaces and critical public facilities in the main urban area were flooded."

3.4. Population Data Processing

Based on the seventh national population census at the township/subdistrict level, a 100 m grid was employed to spatially disaggregate the population across the eight central districts, extracting both total population and age-structure composition (0-14, 15-64, and 65+years) for each grid cell. The total population of the study area is approximately 6.43 million, comprising approximately 1.145 million children (0-14 years, 17.81%), 4.803 million adults (15-64 years, 74.69%), and 0.490 million elderly (65+ years, 7.61%). Given the prohibitive computational burden of simulating the full population, a spatially proportional subsample was extracted based on district-level distributions, ultimately yielding 12,714 simulated evacuees. Shelter capacities were scaled down proportionally correspondingly.

3.5. Evacuation Scenarios and Performance Metrics

Under the most severe 6-hour rainfall period (15:00–20:00 on July 20), three evacuation initiation timings were established: 0 hours (Figure 4.), 1 hour (Figure 5.), and 2 hours (Figure 6.) after rainfall onset. Evacuees were initially positioned within 5 km of shelters, with an average distance to shelters of 4.6 km. To evaluate the impact of deep reinforcement learning on evacuation efficiency under continuously rising water levels, the traditional A* algorithm was employed as the control group under identical scenarios. Two performance metrics were defined: (1) average evacuation time, calculated as the mean evacuation duration across successfully evacuated individuals in each simulation run; and (2) the safety index F, which assigns a score to each traversed path segment based on water depth (shallower water yielding higher scores, with a maximum of 1 and decreasing as depth increases). After each simulation, the F-score for each evacuee was computed as a weighted average over all traversed segments, and a second-stage weighting was applied across all evacuees to obtain the aggregate F-value. A higher F-value indicates a safer evacuation route. An F-value below 0.5 signifies that the agent encountered multiple deep-water segments during evacuation, implying substantial instability risk.

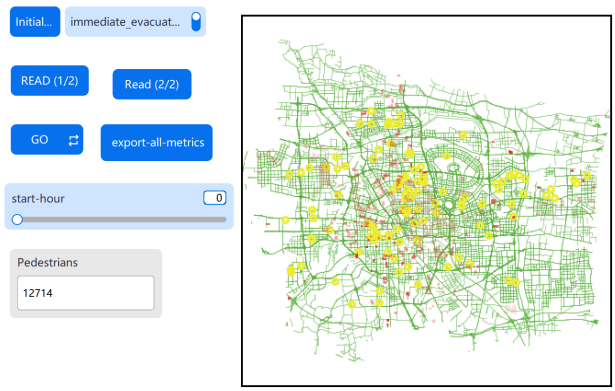


Figure 4. Evacuation scenario at 0 hours after rainfall

(yellow dots denote shelters, red dots denote evacuee agents)

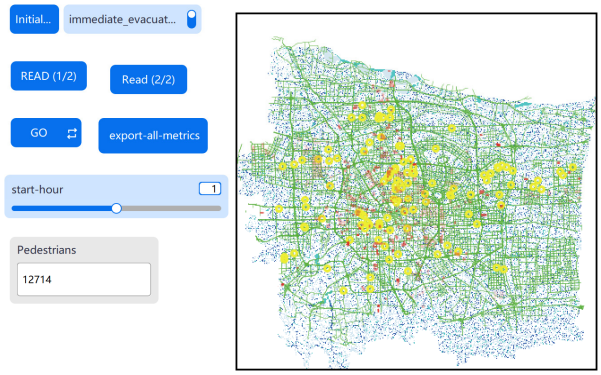


Figure 5. Evacuation scenario at 1 hour after rainfall

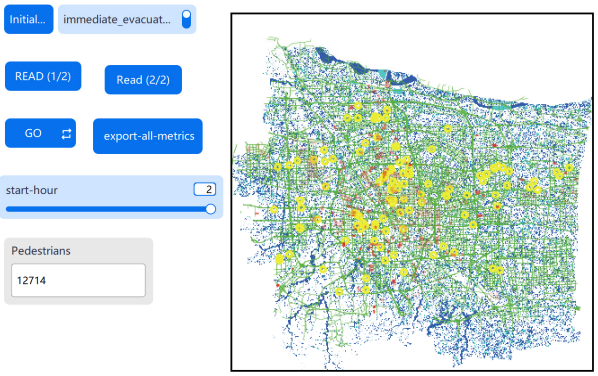


Figure 6. Evacuation scenario at 2 hours after rainfall

4. SIMULATION RESUITS AND DISCUSSION

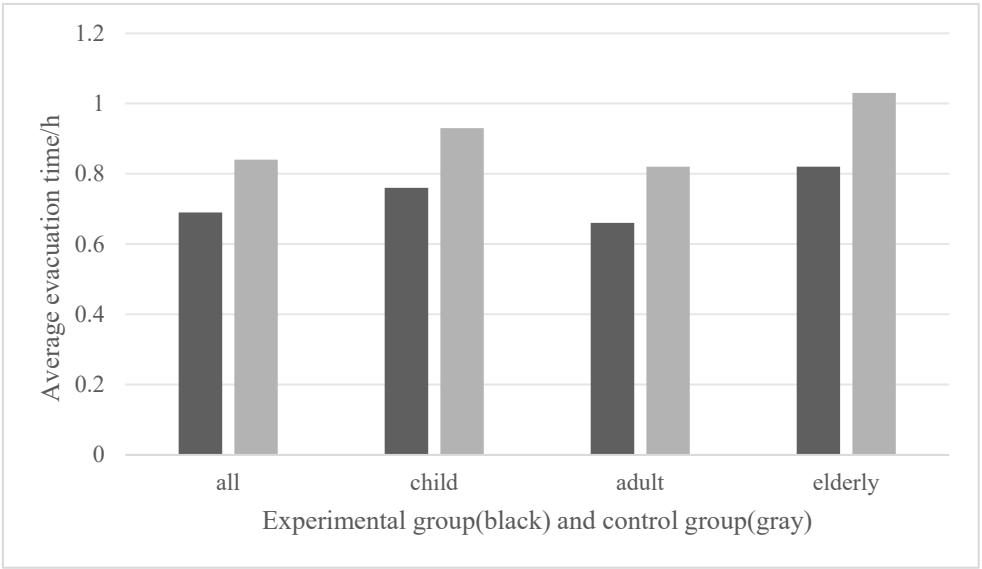


Figure 7. Average evacuation times for Scenario 1—experimental vs. control groups

Scenario 1 (Evacuation Initiated 0 Hours After Rainfall Onset): Evacuation was initiated at 15:00, i.e., immediately upon rainfall commencement. Under this scenario, urban inundation developed relatively slowly, road network capacity declined gradually, and agents faced the lowest risk. The experimental group (agents following DQN-trained evacuation routes) successfully evacuated 12,714

individuals, achieving a 100% evacuation rate; the control group evacuated 12,598 individuals, corresponding to a 99% evacuation rate. The average evacuation times are shown in Figure 7.. The experimental group reduced the overall average evacuation time by approximately 17.8% relative to the control group, with reductions of approximately 18.3% and 20.4% for children and the elderly, respectively.

Scenario 2 (Evacuation Initiated 1 Hour After Rainfall Onset): Evacuation was initiated at 16:00, i.e., 1 hour after rainfall commencement. At this stage, urban inundation had intensified, and agents were required to plan within flooded environments. The experimental group successfully evacuated all 12,714 individuals (100% evacuation rate), whereas the control group evacuated 12,034 individuals (94% evacuation rate). As shown in Figure 9, the experimental group reduced the overall average evacuation time by approximately 37.6% relative to the control group, with reductions of approximately 41.5% and 42% for children and the elderly, respectively.

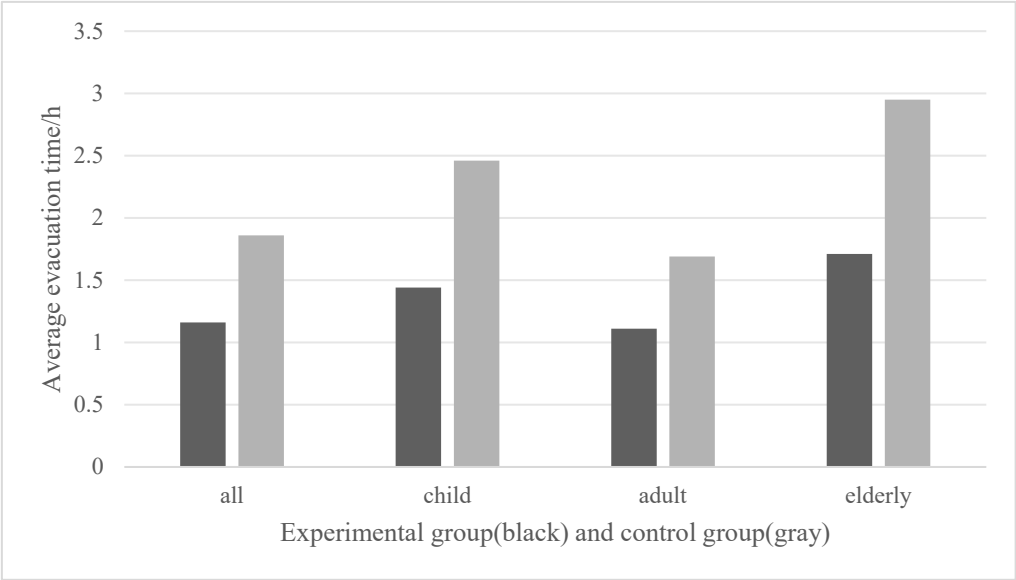


Figure 8. Average evacuation times for Scenario 2—experimental vs. control groups

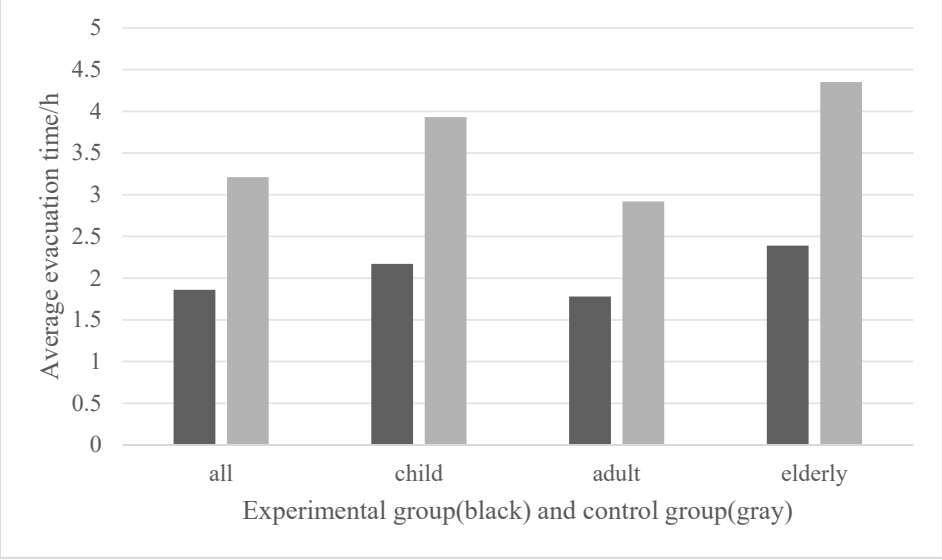


Figure 9. Average evacuation times for Scenario 3—experimental vs. control groups

Scenario 3 (Evacuation Initiated 2 Hours After Rainfall Onset): Evacuation was initiated at 17:00, i.e., 2 hours after rainfall commencement. At this point, rainfall intensity peaked, widespread urban

inundation had developed, and road networks were severely compromised, exposing agents to substantially higher safety risks. The experimental group successfully evacuated 12,621 individuals (99% evacuation rate), while the control group evacuated 11,324 individuals (89% evacuation rate). With rising initial water depths, a small number of experimental-group agents situated in deep-water zones at their starting locations failed to evacuate, whereas the majority of control-group failures resulted from entrapment in deep water along shortest-path routes. The average evacuation times are presented in Figure 10. The experimental group reduced the overall average evacuation time by approximately 42.1% relative to the control group, with reductions of approximately 44.8% and 45.1% for children and the elderly, respectively. As ambient water depth continued to rise, the advantages of the DQN-optimized routes became increasingly pronounced, particularly for children and the elderly—the populations most susceptible to water-depth effects.

The F-values of evacuation outcomes are presented in Figures 11–13. In Scenario 1, the F-values for children and the elderly in the experimental group exceeded those of the control group by approximately 0.21. As simulation water depths progressively increased, F-values declined in both groups; however, the experimental group exhibited a more stable decline. Even when evacuation was initiated 2 hours after rainfall onset, the F-values for children and the elderly in the experimental group remained at 0.78—0.3 higher than those of the control group—indicating that the safety of DQN-planned evacuation routes is highly reliable, with the improvement becoming more pronounced under deep-water conditions. In the control group, F-values for children declined from 0.74 to 0.41, and for the elderly from 0.73 to 0.40—both representing approximately 44.6% and 45.2% decreases—suggesting that shortest-path-based routes expose evacuees to severe instability risks as rainfall persists.

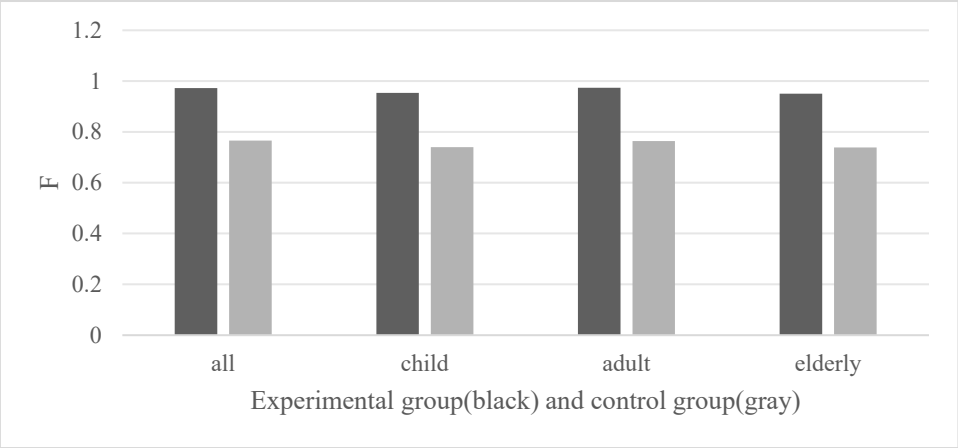


Figure 10. F-values for Scenario 1—experimental vs. control groups

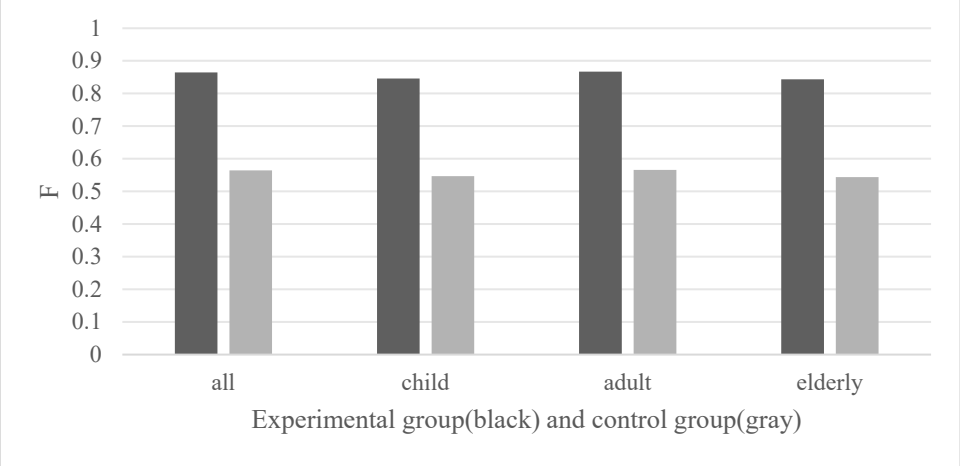


Figure 11. F-values for Scenario 2—experimental vs. control groups

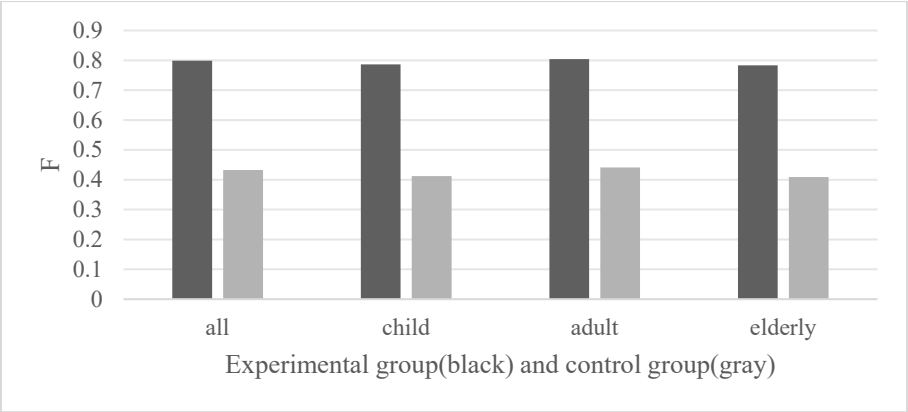


Figure 12. F-values for Scenario 3—experimental vs. control groups

5. CONCLUSION AND OUTLOOK

This study couples ABM simulation with deep reinforcement learning to perform iterative route optimization under multiple constraints, including pedestrian heterogeneity, evacuation efficiency, and path safety. Using the 2021 extreme rainstorm and flood disaster in Zhengzhou as an empirical case, we constructed multi-scenario evacuation simulation experiments and compared the proposed method against the traditional A* algorithm. The following conclusions are drawn: (1) DQN-iteratively optimized evacuation routes significantly enhance evacuation efficiency, with the improvement becoming more pronounced under escalating risk conditions. (2) The dynamically planned routes derived from DQN substantially improve path safety; as surface water accumulation rises, F-values remain within a relatively high range, exhibiting notably greater safety than A*-planned routes. (3) The DQN-trained evacuation routes demonstrate particular advantages for high-risk groups—children and the elderly—with marked improvements in both evacuation efficiency and path safety. These findings offer valuable insights for optimizing urban flood emergency plans and enhancing evacuation response capabilities.

Urban rainstorm flood emergency evacuation is a complex dynamic process characterized by considerable uncertainty and spatiotemporal variability. This study has several limitations that warrant further investigation: (1) Pedestrian movement speed settings could be refined by incorporating blocking factors to more realistically reflect the risk states of evacuees, thereby enabling a more scientifically grounded F-value. (2) The siting and distribution of urban shelters should be further rationalized to ensure that remote areas possess adequate disaster resilience capacity. (3) This study did not address evacuation from high-risk zones; future work should focus on emergency evacuation modeling for critical urban infrastructure (e.g., subway systems) and underground spaces (e.g., tunnels) under extreme rainstorm flood impacts. Additionally, in light of climate change and urbanization, future studies should consider projected changes in extreme precipitation and urban population distribution to conduct evacuation research under future scenarios, thereby providing a robust scientific foundation for urban flood risk management.

REFERENCES

[1] Liu, J. H., Mei, C., Liu, H. W., Fang, X. Y., Ni, G. H., & Jin, W. B. (2023). Key scientific and technical issues in joint prevention and control of external flood and internal waterlogging disaster chains in mega-cities. Advances in Water Science, 34(2), 172–181.

[2] IPCC. (2021). Climate Change 2021: The Physical Science Basis. Summary for Policymakers. Cambridge University Press.

[3] Lu, X. C., Xu, Z. X., Shi, Q. M., et al. (2025). Evolution characteristics and disaster reduction pathways of urban rainstorm-flood disaster chains. Advances in Water Science, 36(1), 97–108.

[4] Lei, N., Zhou, Z. Z., Lu, P., & Liu, S. G. (2025). Non-stationarity and spatiotemporal heterogeneity of extreme precipitation in the Yangtze River Delta under changing environments. Advances in Water Science, 36(3), 436–449.

[5] Xu, Z. X., Ye, C. L., & Liao, R. T. (2023). Collaborative governance of urban flood disasters: Research progress and application cases. Advances in Earth Science, 38(11).

[6] Song, X. M., Zhang, J. Y., Wang, G. Q., He, R. M., & Wang, X. J. (2014). Development and challenges of urban hydrology under changing environments—Part II: Urban stormwater simulation and management. Advances in Water Science, 25(5), 752–764.

[7] Song, X. M., Xu, N. T., Zhang, J. Y., & He, R. M. (2024). Urban flooding in China: Current status, causes, and challenges. Advances in Water Science, 35(3), 357–373.

[8] Zhang, K. H., Mei, C., Liu, J. H., Wang, J., Song, T. X., & Shi, H. Y. (2025). Urban flood identification and simulation verification based on social media big data. Advances in Water Science, 36(4), 566–580.

[9] Li, M. Y., Wang, J., & Shen, H. (2016). Optimization of evacuation route planning algorithms for flood emergencies. Journal of Geo-Information Science, 18(3), 362–368.

[10] He, M., Chen, C., Zheng, F., Chen, Q., Zhang, J., Yan, H., & Lin, Y. (2021). An efficient dynamic route optimization for urban flooding evacuation based on Cellular Automata. Computers, Environment and Urban Systems, 87, 101622. https://doi.org/10.1016/j.compenvurbsys.2021.101622.

[11] Yan, Q. L., Du, E. H., & Zheng, C. M. (2023). Emergency evacuation simulation for urban flood disasters and its efficiency-equity trade-off analysis. Advances in Water Science, 34(3), 409–417.

[12] Kaynak, S., Kaynak, B., Mermer, O., & Demir, I. (2025). City-scale digital twin framework for flood impact analysis: Integrating urban infrastructure and real-time data analytics.

[13] Lee, H. K., Hong, W. H., & Lee, Y. H. (2019). Experimental study on the influence of water depth on the evacuation speed of elderly people in flood conditions. International Journal of Disaster Risk Reduction, 39, 101198. https:// doi. org/10.1016/j.ijdrr.2019.101198.

[14] Shi, D., Li, J., Wang, Q., Chen, J., Lovreglio, R., Lo, J. T., & Ma, J. (2025). Modeling and simulation of crowd dynamics at evacuation bottlenecks during flood disasters. Transportation Research Part E: Logistics and Transportation Review, 198, 104064. https://doi.org/10.1016/j.tre.2025.104064.

[15] Takabatake, T., Asai, K., Kakuta, H., & Hasegawa, N. (2025). Optimizing evacuation paths using agent-based evacuation simulations and reinforcement learning. International Journal of Disaster Risk Reduction, 117, 105173. https://doi.org/10.1016/j.ijdrr.2025.105173.

[16] Bernardini, G., & Quagliarini, E. (2020). How to account for the human motion to improve flood risk assessment in urban areas. Water, 12(5), 1316. https://doi.org/10.3390/w12051316.

[17] Zhuang, X., & Wu, C. (2018). Display of required crossing speed improves pedestrian judgment of crossing possibility at clearance phase. Accident Analysis & Prevention, 112, 15–20. https://doi.org/ 10. 1016/ j. aap. 2017. 12. 014.

[18] Shirvani, M., & Kesserwani, G. (2021). Flood–pedestrian simulator for modelling human response dynamics during flood-induced evacuation: Hillsborough stadium case study. Natural Hazards and Earth System Sciences, 21(10), 3175–3198. https://doi.org/10.5194/nhess-21-3175-2021.

[19] Shang, W., Wu, Z. Y., Zheng, W., Zeng, Y. J., & Lü, S. (2021). Study on the correlation between street attractiveness and the rate of change of walking speed in modern cities. Architectural Journal, 68, 99–105.

[20] Shang, W., Wu, Z., Zheng, W., Zeng, Y., & Lv, S. (2021). Study on the correlation between street attractiveness and the rate of change of walking speed in modern cities. Architectural Journal, 68, 99–105.

[21] Sharbaf, M., Bélanger, V., Cherkesly, M., Rancourt, M. È., & Toglia, G. M. (2025). Risk-based shelter network design in flood-prone areas: An application to Haiti. Omega, 131, 103194. https://doi.org/ 10.1016/ j. omega. 2024. 103194.

[22] Wang, H. L., Yan, D. M., Liu, H. W., Wu, Z. N., & Zhou, Y. H. (2026). Dynamic personalized emergency evacuation route planning methodology and application for urban flooding. Advances in Water Science, 37(3), 465–479.

[23] Xia, X., & Ming, X. (2025). SynxFlow: A GPU-accelerated Python package for multi-hazard simulations. Journal of Open Source Software, 10(111), 7586. https://doi.org/10.21105/joss.07586.

[24] Su, P., Xu, W., Ming, X., Gu, Z., & Xia, G. (2026). SynxFlow-based urban pluvial flood simulation and sensitivity evaluation in the central urban area of Shenzhen. Journal of Hydrology: Regional Studies, 65, 103325. https:// doi. org/ 10.1016/j.ejrh.2026.103325.

[25] Disaster Investigation Team of the State Council of the People's Republic of China. (2022). Investigation report on the "7·20" extreme rainstorm disaster in Zhengzhou, Henan Province.

[26] Ministry of Housing and Urban-Rural Development of the People's Republic of China, & General Administration of Quality Supervision, Inspection and Quarantine of the People's Republic of China. (2021). Code for design of disaster prevention shelters (GB 51143-2015).